PHYSICAL REVIEW B VOLUME 23, NUMBER 7 1 APRIL 1981

Stress effects on the electron-spin-resonance spectra of Er in gold and silver thin films

C. A. Pelá, J. F. Suassuna, G. E. Barberis, and C. Rettori
Instituto de Física "Gleb Wataghin," Universidade Estadual de Campinas, 13100, Campinas, S. P., Brasil
(Received 17 June 1980)

Electron-spin-resonance measurements were carried out at liquid-helium temperatures on diluted Er in Au and Ag thin films (300–5000 Å) evaporated on NaCl and quartz substrates. The observed anisotropy of the g value, linewidth, and line shape are explained by the mixing of excited crystalline field levels with the Γ_7 ground state: these admixtures are caused by the stresses induced by the difference between the thermal expansion coefficients of the substrate and the film. Lower limits for the tetragonal and trigonal second-order orbit-lattice coupling parameters can be estimated from the data. In Au their magnitude and sign agree with those predicted by the point-charge model, while in Ag the trigonal parameter does not. Qualitative information about the strain distribution across the film was obtained by employing the anisotropy of the g value, the linewidth, and the line shape together with x rays and electron-microscopy analysis.

I. INTRODUCTION

To understand the spin-lattice relaxation mechanism, the orbit-lattice coupling parameters (OLCP) have been measured in many stress experiments performed in the past two decades on non-S-state ions in insulators,[1–3] but only recently have a few works been reported of such effects in metallic hosts.[4–8] The purpose of the present work is to give additional experimental data and a few general conclusions about the effect of stress on the electron-spin-resonance (ESR) spectra of dilute Er in thin films of Au and Ag.

Careful experimental measurements of the anisotropy of the g value, linewidth, and line shape as a function of the thickness and deposition temperatures (i.e., deformation) of the film, enabled us to gain some information about the magnitude and distribution of the strain across the film.

We show that it will be possible to extract from these experiments a lower limit for the tetragonal and trigonal second-order orbit-lattice coupling parameters[4–8] (OLCP). Surprisingly in the case of Au,[5,8] these parameters agree in magnitude and sign with those predicted by the point-charge model (PCM) and are of the same order of magnitude than those measured in equivalent insulating lattices,[1–3] but in the case of Ag (Refs. 4,6, and 7) an "anomaly" was found on the trigonal OLCP: its sign is opposite to that of the Au as well as to the one predicted by the PCM. A similar effect occurs with the fourth-order static crystalline field parameter measured by Williams and Hirst,[9] in Au and Ag.

Section II is concerned with the experimental details, and in Sec. III we give the experimental results. Section IV deals with the theoretical interpretation of these results and in Sec. V we conclude with a general discussion about this work.

II. EXPERIMENTAL TECHNIQUES

The ESR measurements were carried out in a conventional Varian E-line X-Band spectrometer at microwave power levels of 1–10 mW. The data were taken at liquid-helium temperatures (1.5–4.2 K). The cryostat employed is a stainless-steel Dewar[10] with a quartz tail which allows sample rotation and fits into a conventional 100-kHz TE_{102} rectangular Varian cavity that is kept at room temperature.

The films were grown in an ultra-high-vacuum ($\sim 10^{-8}$ Torr) system without backing, on surfaces of 0.5×1 cm^2 of (001)- and (111)-oriented NaCl single crystals and on amorphous quartz. In the case of quartz substrates the surfaces were carefully cleaned with acetone. The (001) NaCl faces were obtained by cleaving the crystal in air and the (111) faces by polishing them. In both cases the surfaces were always washed with water in order to favor epitaxiality.[11] During deposition the substrates were kept at temperatures between 25 and 390 °C, depending upon the type of film required and of the desired deformation. After deposition the film substrate was cooled down to room temperature in about 90 min and no further thermal treatment was done on the films. Following this method, three kind of films were obtained: (a) (001)-oriented single crystalline films on a hot (~ 350 °C for Ag and ~ 390 °C for

Au) (001) NaCl substrate, (b) (111)-oriented single crystalline films on a hot (~300 °C for Ag and ~350 °C for Au) (111) NaCl substrate, and (c) (111)-oriented films, with mosaic structure, i.e., many microcrystals, all of them oriented with their [111] direction along the direction perpendicular to the plane of the film and with their other directions at random. This kind of structure was always obtained on cold or hot quartz substrates and even on (001) or (111) NaCl substrates as long as the deposition temperature was maintained below 200 °C for Ag and 250 °C for Au.

The films were always evaporated from the alloys with 1 to 2% of nominal Er concentration, previously prepared in a conventional arc furnace. It was observed that a high deposition rate (~600 Å/sec) improved the impurity homogeneity in the film. We found that even though the vapor pressure of the rare earth is higher than that of the noble metals, most of the rare earth does not evaporate until the end for evaporation rates of 10 to 100 Å/sec. We have arrived at this conclusion because in films evaporated at a slow rate from the same alloy, those which were evaporated later, showed stronger ESR line intensities; some demagnetization effects could also be detected in these films. Therefore we got better results on films where all of the material necessary for a required thickness was evaporated as fast as possible, i.e., by flashing it out. We noticed that a fast evaporation required higher deposition temperature of the substrates in order to get good epitaxiality. The thickness of the films was conventionally determined by measuring the shift in the frequency of a quartz oscillator.

When it was necessary to release the film from the substrate, for resonance experiments or electron-microscopy analyses, the NaCl and quartz substrates were dissolved in water and fluoridric acid, respectively. Once the substrate was completely dissolved, the film floated on the surface of the liquid, and it was then transported to a Teflon tape for the required experiment.

The x-ray analyses were done in a conventional x-ray diffractometer. From the intensity of the film's diffraction lines it was possible to get a quantitative idea about the overall preferential orientation of the film, and from a "rocking curve" of these lines, the angular dispersion of the preferential orientation was also obtained. With the preparation method described above, we were always able to get better than 95% (001)- or (111)-oriented films with a maximum dispersion of 2%. The films with mosaic structure showed bigger dispersion, indicating a little misorientation of the [111] direction of the microcrystals with respect to the direction perpendicular to the film. In the case of quartz substrate this effect was found to be even bigger (~5%) for films evaporated at room temperatures.

Films thinner than 1500 Å were also analyzed with a conventional Hitachi 120-kV electron microscope. The results always confirmed the x-ray and ESR conclusions. These analyses gave additional support to the interpretation of the ESR data for very thin Au films (< 600 Å), where a cracking of the film was assumed (see below) in order to understand the absence of anisotropies in the ESR spectra.

III. EXPERIMENTAL RESULTS

The ground level of dilute Er in bulk Au and Ag has already been found to be a doublet Γ_7.[12,13] In a few cases we have also separated the film from the substrate and measured them again. We have then found that the g value, thermal broadening of the linewidth, and hyperfine constants agree, within the experimental accuracy, with those obtained in bulk.[12,13] Therefore we conclude that the observed resonance actually comes from Er diluted in Au and Ag films.

Since the data depend strongly on the film's growing conditions, like thickness, substrate, surface, deposition temperature, etc., we have done experiments on a large number of films, grown under different conditions in order to get more systematic data.

The general behavior of the measurements can be summarized as follows:

(i) The g values of the resonances show an anisotropy which can be fitted to the following formula

$$g(\theta) = g_0 + \tfrac{1}{2}\Delta g\,(3\cos^2\theta - 1) \quad . \tag{1}$$

(ii) In many cases the linewidth of the resonances show an anisotropy which could be fitted to the following formula:

$$\Delta H(\theta) = \Delta H_0 + \tfrac{1}{2}\Delta H_1 |3\cos^2\theta - 1| \quad . \tag{2}$$

(iii) In some cases an anisotropy of the line shape was observed and could be approximately fitted to the derivative with respect to the field H of

$$P(H) = \sum_{z=0}^{z=n} \frac{T_2/\pi}{1 + (\gamma T_2)^2 (H - H_{\rm res})^2} \quad , \tag{3}$$

where

$$H_{\rm res} = H_0 \left[1 - \tfrac{1}{2} F(z) \frac{\Delta g}{g} (3\cos^2\theta - 1) \right] \quad .$$

In Eqs. (1), (2), and (3), g_0, Δg, ΔH_1 are fitting parameters. T_2 is the transverse relaxation time, n is twice the number of lattice constants making up the thickness of the film, $\gamma = g\mu_B/\hbar$, and

$$F(z) = \epsilon_{i\alpha}(z)/\epsilon_{i\alpha}(z=0)$$

(see below) is a function which takes into account the nonuniformity of the normal strains across the

film, where z is the axis perpendicular to the plane of the film.

When Eqs. (1)–(3) are employed to describe the measurements a different behavior is shown by the Au:Er and Ag:Er films. In consequence we are going to present them separately.

A. Au:Er films

Figure 1 shows a typical ESR spectra of Er in a 4700-Å thick film of Au evaporated on a hot (001) NaCl substrate. Figure 2 shows the typical g value and linewidth anisotropies observed in our Au:Er films when the magnetic field is rotated in a plane perpendicular to the plane of the film. The angle is measured from the normal to the plane of the film and the solid lines are the best fit to Eqs. (1) and (2).

The typical line-shape anisotropies observed on Au:Er films having a (111) mosaic structure are shown in Figs. 3 and 4. Figure 3 corresponds to a 680 Å film deposited on a hot (374 °C) quartz substrate and Fig. 4 to a 880 Å film deposited on a cold (140 °C) (001) NaCl substrate. Note that the broadening of the resonance toward lower or higher fields depends upon the sign of Δg as predicted by Eq. (3). The angle θ is again the angle between the normal to the plane and the magnetic field. The dots indicate the best fit of the derivative of Eq. (3) to the experimental spectra: we have tentatively used

$$F(z)=\begin{cases}1, & 0\leq z<a\\ d+\dfrac{(1-d)}{a-c}(z-c), & a\leq z<c\\ d, & c\leq z<\delta\ ,\end{cases}\qquad(4)$$

where a, c, d, and Δg are fitting parameters and δ the thickness of the film. The inserts are the best $F(z)$ functions which fit the data of Figs. 3 and 4.

Table I gives the parameters that fit Eqs. (1) and (2) to the experimental data for each of the analyzed Au:Er films. The thicknesses, deposition temperatures, and expected deformations are also given.

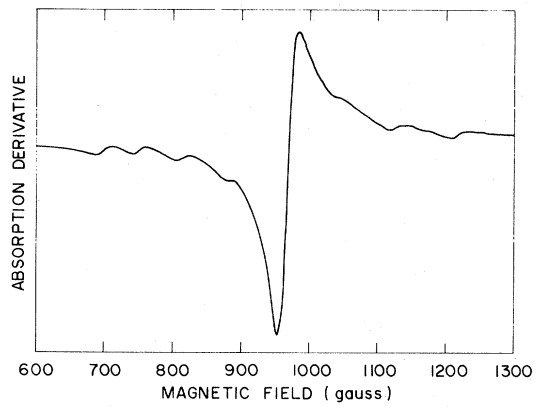

FIG. 1. Typical ESR spectra at 1.5 K of a 4700-Å (001) Au:Er film, evaporated on a hot (385 °C) NaCl substrate.

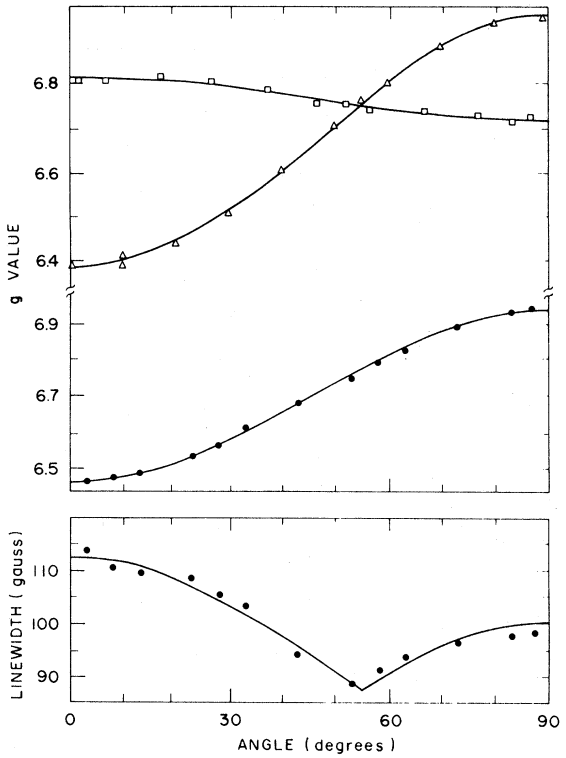

FIG. 2. g value and linewidth anisotropies of Au:Er films at 1.5 K. □ correspond to a 1300-Å (111) film evaporated on a hot (346 °C) (111) NaCl substrate, Δ to a 870-Å (mosaic) film deposited on a hot (320 °C) quartz substrate and ● to a 700-Å (001) film evaporated on a hot (346 °C) (001) NaCl substrate.

It is worthwhile to mention that (a) we have observed line-shape anisotropy only in those films with (111) structure (either single crystal or mosaic) with small or no linewidth anisotropy, and with relatively small total linewidth, (b) for films thinner than 3000 Å the line shape was found to be always symmetric (thickness smaller than twice the skin depth), at $\theta=54.7°$.

Table I shows clearly a dependence of Δg with the film thickness, and a maximum anisotropy of g was found for films of about 550 Å. We believe that this effect can be explained as follows: for films thinner that 550 Å a cracking of the film occurs as a consequence of the applied deformation and the stresses are then partially released. This conclusion is supported by electron-microscopy analyses performed on our samples which show that the thinner the films the more discontinuous they are. On the other hand for films thicker than 900 Å the films are continuous but we believe that they are too thick to accept all the

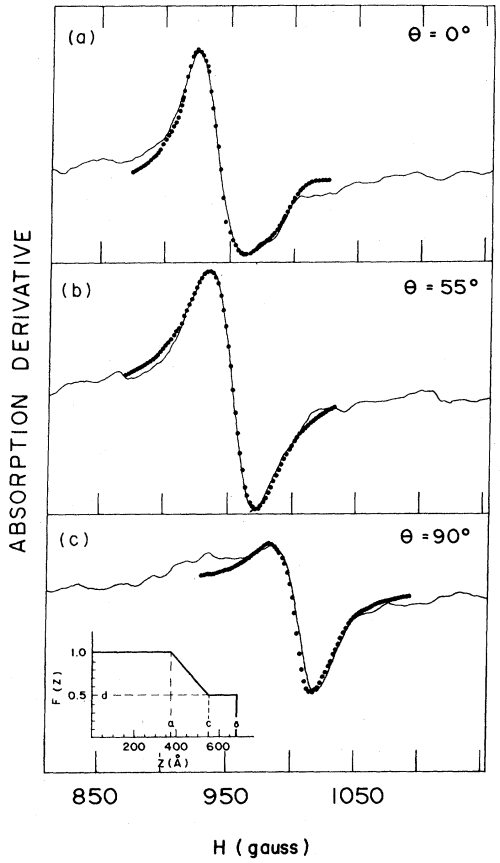

FIG. 3. Line-shape anisotropy at 1.5 K for a 680-Å Au:Er film with (111) mosaic structure, evaporated on a hot (374 °C) quartz substrate. The insert shows the best $F(z)$ function (see text) which fits the experimental line shape (closed circles).

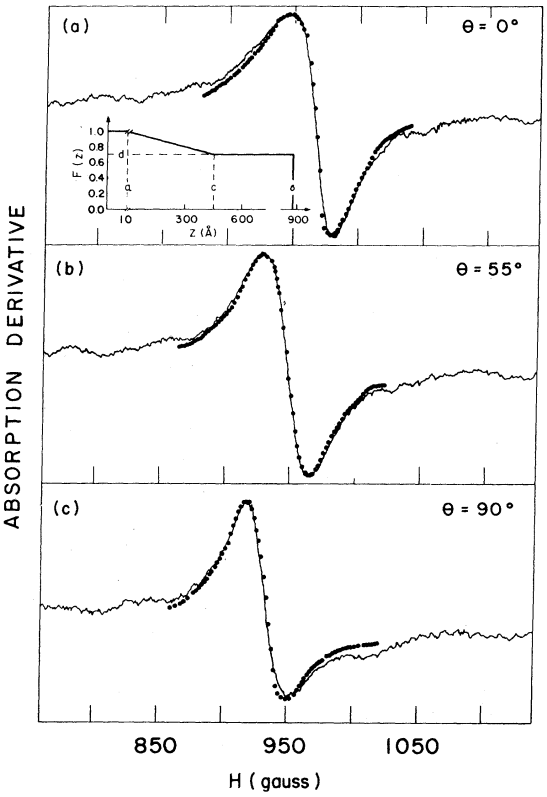

FIG. 4. Line-shape anisotropy at 1.5 K for a 880-Å Au:Er film with (111) mosaic structure, evaporated on a cold (140 °C) (001) NaCl substrate. The insert shows the best $F(z)$ function (see text) which fits the experimental line shape (closed circles).

expected deformation, so that the films partially slide with respect to the substrate. Since the anisotropy of the linewidth does not seem to be larger for thicker films (see Table I) we do not believe that the decrease in the g-value anisotropy could be attributed to a significant increase of the nonuniformity of the deformation across the film.

Another evidence of possible sliding effects of the films is given by the fact that while on (111) NaCl substrates the g-value anisotropy is almost independent of the thickness and deformation (higher deposition temperatures), for quartz substrates it almost scales with the deformation (see Table I).

B. Ag:Er films

Figure 5 shows a typical ESR spectra of Er in a 2300-Å thick film of Ag deposited on a hot quartz substrate. For films thinner than 2000 Å the line

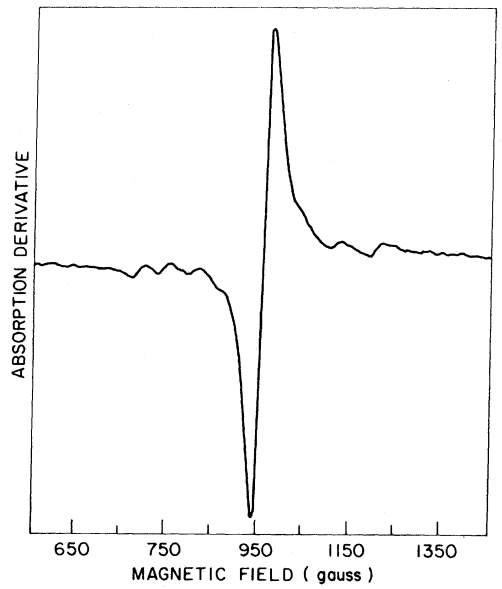

FIG. 5. Typical ESR spectra at 1.5 K of a 2300-Å (mosaic) Ag:Er film, evaporated on a hot (340 °C) quartz substrate.

TABLE I. Experimental ESR data of Au:Er thin films.

Substrate	Thickness[a] δ (Å)	Deposition temperature[a] T_d (°C)	Deformation ϵ'_{xx} (%)	g_0	Δg	ΔH_0[b] (G)	ΔH_1	Film's structure (x ray)	$\langle \Delta \epsilon^2_{i\alpha}(z') \rangle^{1/2} / \langle \epsilon_{i\alpha}(z') \rangle$
	220	380	−1.76	6.78	−0.09	70	· · ·	(001)	· · ·
	350	340	−1.34	6.78	−0.07	35	· · ·	(001)	· · ·
	350	400	−1.84	6.76	−0.11	40	14	(001)	0.90
	420	375	−1.74	6.76	−0.27	103	54	(001)	1.41
	480	380	−1.76	6.78	−0.16	104	20	(001)	0.89
NaCl (001)	550	280	−1.37	6.76	−0.39	106	39	(001)	0.71
	580	365	−1.70	6.77	−0.35	18	12	(001)	0.24
	700	345	−1.62	6.77	−0.31	87	25	(001)	0.57
	1000	310	−1.48	6.77	−0.29	25	13	(001)	0.31
	3000	310	−1.48	6.77	−0.19	12	5	(001)	0.18
	3500	400	−1.84	6.77	−0.13	80	· · ·	(001)	· · ·
	4700	385	−1.78	6.78	−0.09	30	· · ·	(001)	· · ·
	300	345	−1.62	6.77	0.02	40	· · ·	(111)	· · ·
	435	345	−1.62	6.78	0.04	52	· · ·	(111)	· · ·
	550	345	−1.62	6.77	0.07	55	· · ·	(111)	· · ·
	638	330	−1.56	6.78	0.02	100	· · ·	(111)	· · ·
	650	315	−1.50	6.78	0.11	55	· · ·	(111)	· · ·
	800	345	−1.62	6.77	0.03	90	· · ·	(111)	· · ·
	870	320	−1.52	6.78	0.02	70	· · ·	(111)	· · ·
NaCl (111)	1000	30	−0.54	6.78	0.02	70	· · ·	(111)[c]	· · ·
	1000	340	−1.60	6.77	0.07	70	· · ·	(111)	· · ·
	1300	345	−1.62	6.77	0.07	50	· · ·	(111)	· · ·
	2200	345	−1.62	6.78	0.05	40	· · ·	(111)	· · ·
	2200	345	−1.62	6.77	0.03	70	· · ·	(111)	· · ·
	3300	370	−1.72	6.78	0.05	30	· · ·	(111)	· · ·
	300	345	0.80	6.78	−0.14	20	· · ·	(111)[c]	· · ·
	320	370	0.83	6.79	−0.03	47	· · ·	(111)[c]	· · ·
	550	345	0.80	6.77	−0.28	32	· · ·	(111)[c]	· · ·
	640	330	0.78	6.77	−0.31	44	56	(111)[c]	1.28
	680	375	0.84	6.78	−0.24	35	· · ·	(111)[c]	· · ·
	800	345	0.80	6.77	−0.38	32	· · ·	(111)[c]	· · ·
	870	320	0.76	6.79	−0.38	35	· · ·	(111)[c]	· · ·
Quartz	1000	30	0.31	6.78	−0.10	60	· · ·	(111)[c]	· · ·
	1000	210	0.61	6.79	−0.24	40	· · ·	(111)[c]	· · ·
	1000	340	0.79	6.78	−0.41	42	· · ·	(111)[c]	· · ·
	1250	30	0.31	6.78	−0.08	40	· · ·	(111)[c]	· · ·
	1300	120	0.46	6.77	−0.20	20	· · ·	(111)[c]	· · ·
	1650	340	0.79	6.77	−0.30	35	· · ·	(111)[c]	· · ·
	2200	345	0.80	6.77	−0.28	28	12	(111)[c]	0.30
	3300	370	0.83	6.78	−0.21	25	14	(111)[c]	0.47
	4300	30	0.31	6.78	−0.12	70	· · ·	(111)[c]	· · ·
	4300	340	0.79	6.78	−0.37	45	· · ·	(111)[c]	· · ·
	4900	340	0.79	6.77	−0.15	21	5	(111)[c]	0.23
	660	195	−1.05	6.77	0.18	12	· · ·	(111)[c]	· · ·
	770	220	−1.15	6.76	0.20	20	· · ·	(111)[c]	· · ·
NaCl (001)	880	140	−0.88	6.79	0.15	35	· · ·	(111)[c]	· · ·
	1200	30	−0.54	6.78	0.17	18	· · ·	(111)[c]	· · ·
	1500	330	−1.56	6.77	0.14	35	· · ·	(111)[c]	· · ·

[a]The thicknesses and deposition temperatures are determined within 10%.

[b]The linewidths are determined within 10–15% of accuracy.

[c]Mosaic structure.

TABLE II. Experimental ESR data of Ag:Er thin films.

Substrate	Thickness[a] δ (Å)	Deposition temperature T_0 (°C)	Deformation ϵ'_{xx} (%)	g_0	Δg	ΔH_0[b] (G)	ΔH_1	Film's structure (x ray)	$\langle \Delta \epsilon_{i\alpha}^2(z') \rangle^{1/2} / \langle \epsilon_{i\alpha}(z') \rangle$
	1300	380	−1.63	6.82	−0.05	28	···	(001)	···
NaCl (001)	1600	355	−1.54	6.81	−0.05	32	···	(001)	···
	3500	375	−1.61	6.81	−0.07	60	···	(001)	···
	320	280	−1.27	6.82	−0.23	38	16	(111)	0.50
	540	270	−1.24	6.82	−0.30	47	18	(111)	0.43
	680	305	−1.38	6.80	−0.30	42	35	(111)	0.83
	1000	305	−1.38	6.79	−0.33	41	44	(111)	0.95
	1400	305	−1.38	6.80	−0.29	95	35	(111)	0.86
	2000	300	−1.36	6.78	−0.28	20	5	(111)	0.12
NaCl (111)	2100	310	−1.39	6.78	−0.26	50	26	(111)	0.71
	2300	30	−0.44	6.78	−0.22	81	14	(111)[c]	0.45
	2300	185	−0.98	6.80	−0.28	140	···	(111)[c]	···
	2300	340	−1.49	6.78	−0.31	78	···	(111)	···
	3850	310	−1.39	6.78	−0.33	53	47	(111)	1.01
	220	305	0.99	6.79	0.14	65	···	(111)[c]	···
	420	305	0.99	6.80	0.21	42	24	(111)[c]	0.82
	680	305	0.99	6.81	0.16	80	···	(111)[c]	···
	950	300	0.98	6.80	0.21	76	35	(111)[c]	1.19
	1000	60	0.52	6.78	0.21	60	···	(111)[c]	···
	1000	305	0.98	6.84	0.17	110	···	(111)[c]	···
Quartz	1400	305	0.98	6.85	0.16	130	···	(111)[c]	···
	2100	310	1.00	6.80	0.12	60	16	(111)[c]	0.95
	2300	30	0.46	6.78	0.18	90	···	(111)[c]	···
	2300	340	1.06	6.81	0.18	134	···	(111)[c]	···
	3850	310	1.00	6.83	0.18	117	13	(111)[c]	0.52
	1000	30	−0.44	6.78	−0.17	120	33	(111)[c]	1.36
	1600	30	−0.44	6.80	−0.25	69	28	(111)[c]	0.78
NaCl (001)	2400	280	−1.27	6.80	−0.36	35	···	(111)[c]	···
	4200	280	−1.27	6.80	−0.12	52	5	(111)[c]	0.30

[a]The thicknesses and deposition temperatures are determined within 10%.
[b]The linewidths are determined within 10–15% of accuracy.
[c]Mosaic structure.

shape was found to be always symmetric.

Figure 6 shows the typical g value and linewidth anisotropies observed on our Ag:Er thin films evaporated on quartz and (001) and (111) NaCl substrates when the magnetic field is rotated in a plane perpendicular to the plane of the film. The solid lines are the best fit to Eqs. (1) and (2).

None of the Ag:Er films have shown an observable line-shape anisotropy, but on the other hand most of them have shown linewidth anisotropies, except those with a (001) structure.

Table II gives the parameters that fit Eqs. (1) and (2) to the experimental data, for each of the analyzed Ag:Er films. We also give the thicknesses, deposition temperature, and expected deformation.

Table II shows that the g-value anisotropy for NaCl and quartz substrates is almost independent of the film thickness. On the other hand, while the g-value anisotropy almost scales with the deformation for hot (111) NaCl substrates, this is not the case for quartz substrates, indicating again that the film could have partially slid off the substrate.

In conclusion we can say that according to our data and interpretation the Au films stick more strongly on quartz than on NaCl and that the inverse is valid for Ag films.

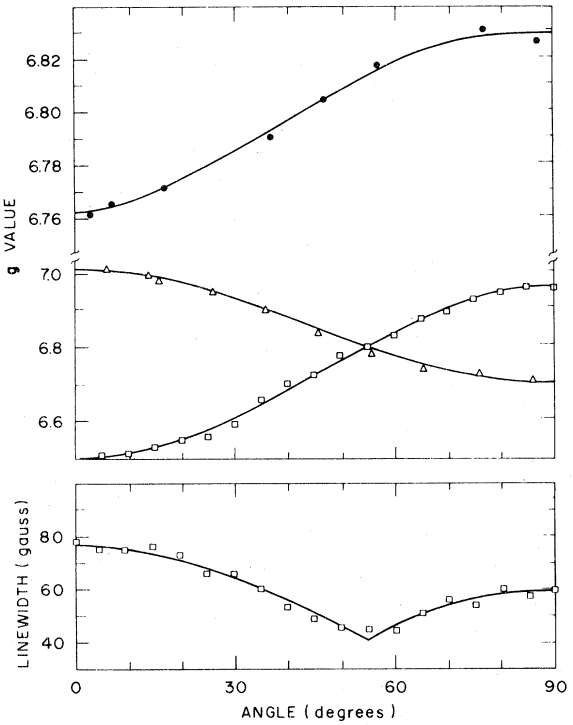

FIG. 6. g value and linewidth anisotropies of Ag:Er films at 1.5 K. ● correspond to a 1600-Å (001) film evaporated on a hot (355 °C) (001) NaCl substrate, Δ to a 950-Å (mosaic) film deposited on a hot (298 °C) quartz substrate, and □ to a 680-Å (111) film evaporated on a hot (305 °C) (111) NaCl substrate.

IV. ANALYSIS

The anisotropy of the g value can be interpreted in terms of a planar strain induced on the film by the difference in thermal expansion coefficients $[\alpha(T)]$ between the film and substrate. This planar deformation will admix the excited $\Gamma_8^{(i)}$ levels into the Γ_7 ground state.

The induced planar strains can be calculated by

$$\epsilon'_{xx}=\epsilon'_{yy}=\int_{T_m}^{T_d}[\alpha_{\text{film}}(T)-\alpha_{\text{subst}}(T)]\,dT \quad , \tag{5}$$

where ϵ'_{ij} are the components of the strain tensor; we chose the interface as the x',y' plane, and indicate with T_m and T_d the measurement and deposition temperatures, respectively. ϵ'_{zz} can be obtained from Eq. (5) and the elastic compliances (S_{ij}) for gold and silver. These compliances and the thermal expansion coefficients are tabulated in Ref. 14.

In the spin-lattice Hamiltonian formalism the stress-induced g shift for (001)- and (111)-planar strain can be written as[2,3]

$$g(\theta)=g_{ff}+g_{1g}\epsilon_{1g}+\tfrac{1}{2}g_{3g}\epsilon_{3g\theta}(3\cos^2\theta-1) \tag{6}$$

and

$$g(\theta)=g_{ff}+g_{1g}\epsilon_{1g}+\tfrac{1}{2}g_{5g}\epsilon_{5g}(3\cos^2\theta-1) \quad , \tag{7}$$

respectively, where g_{ff} is the g value of the free film (or the bulk g value). The normal strains $\epsilon_{i\alpha}$ at the interface are

$$\epsilon_{1g}=\epsilon_{xx}+\epsilon_{yy}+\epsilon_{zz} \quad , \tag{8}$$

$$\epsilon_{3g\theta}=\tfrac{1}{2}(2\epsilon_{zz}-\epsilon_{xx}-\epsilon_{yy})=(\alpha-1)\epsilon'_{xx} \quad , \tag{9}$$

$$\epsilon_{5g}=\epsilon_{5g\chi}=\epsilon_{5g\lambda}=\epsilon_{5g\omega}=\frac{\sqrt{3}}{3}(\beta-1)\epsilon'_{xx} \quad , \tag{10}$$

where

$$\alpha=\frac{2S_{12}}{S_{11}+S_{12}}=\frac{\epsilon'_{zz}}{\epsilon'_{xx}}$$

for (001) films and

$$\beta=\frac{2(S_{11}+2S_{12}-S_{44})}{2S_{11}+4S_{12}+S_{44}}=\frac{\epsilon'_{zz}}{\epsilon'_{xx}}$$

for (111) films. The ϵ_{ij} are the components of the strain tensor referred to the film's cubic axis. For [001]-oriented films, $\epsilon_{ij}=\epsilon'_{ij}$, but for [111]-oriented films ϵ_{ij} and ϵ'_{ij} are related by a rotation of the axis.[7]

The g value of the free film (g_{ff}) and the experimental parameter g_0, that was obtained by fitting the data to Eq. (1), coincides within the experimental error (see Tables I and II). The effects of hydrostatic compression or expansion which could induce admixtures with other J multiplets can therefore be ignored.

A nonuniform stress distribution across the film would lead to the following expressions for the measured g value and linewidth

$$g(\theta)=g_{ff}+\tfrac{1}{2}g_{3g}\langle\epsilon_{3g\theta}(z')\rangle(3\cos^2\theta-1) \quad , \tag{11}$$

$$\Delta H(\theta)=\Delta H_0+\tfrac{1}{2}H_0(g_{3g}/g_{ff})\times\langle\Delta\epsilon^2_{3g\theta}(z')\rangle^{1/2}|3\cos^2\theta-1| \quad , \tag{12}$$

for [001]-oriented films and

$$g(\theta)=g_{ff}+\tfrac{1}{2}g_{5g}\langle\epsilon_{5g}(z')\rangle(3\cos^2\theta-1) \quad , \tag{13}$$

$$\Delta H(\theta)=\Delta H_0+\tfrac{1}{2}H_0(g_{5g}/g_{ff})\times\langle\Delta\epsilon^2_{5g}(z')\rangle^{1/2}|3\cos^2\theta-1| \quad , \tag{14}$$

for [111]-oriented films. Here $\langle\epsilon_{3g\theta}(z')\rangle$ and $\langle\epsilon_{5g}(z')\rangle$ are the mean values and $\langle\Delta\epsilon^2_{3g\theta}(z')\rangle^{1/2}$ and $\langle\Delta\epsilon^2_{5g}(z')\rangle^{1/2}$ the dispersion of the spatial strain distribution along the axis perpendicular to the film (z' axis). Although Eqs. (11) to (14) are only an approximation (see Ref. 4), they show the appropriate experimental angular dependence given by Eqs. (1) and (2). The g value and linewidth could only be cal-

culated from the spectra if the effect of the actual spatial strain distribution on the line shape were known. Within our experimental signal-to-noise ratio a line-shape anisotropy was observed only in the case of (111) gold thin films (see above), and the rest of the data was analyzed according to the method of Peter *et al.*[15]

The ratio

$$\langle \Delta\epsilon_{i\alpha}^2(z')\rangle^{1/2}/\langle \epsilon_{i\alpha}(z')\rangle$$

gives an idea of the nonuniformity of the deformation across the film, and is given in Tables I and II only when the anisotropy of the linewidth could be clearly distinguished from the experimental error of the linewidth. This ratio can be calculated from the data fitted by Eqs. (1) and (2), since H_0 and g_{ff} are known.

Assuming that $\langle \epsilon_{3g\theta}(z')\rangle$ and $\langle \epsilon_{5g}(z')\rangle$ take the value of the corresponding normal deformation at the interface obtained from Eq. (5), we can estimate lower limits for g_{3g} and g_{5g}.

For Au:Er a lower limit of the g_{3g} value is obtained from the **550-Å** (001) film which gives the maximum g-value anisotropy (per unit strain). The lower limit of the g_{5g} value is obtained from the **1000-Å films** evaporated on quartz, since they show biggest anisotropies of the g value per unit strain and it seems that the sliding effects are not too important in this case, i.e., the g-value anisotropy, Δg, almost scales with the deformation (see Table I). The calculated values are

$$g_{3g} \geq 8.0 \quad \text{and} \quad g_{5g} \geq 36.8 \ . \tag{15}$$

For Ag:Er a lower limit of the g_{3g} value is obtained from any of the (001) films, since they give similar values. The value of g_{5g} was obtained from the 1600-Å film deposited on cold (30 °C) (001) NaCl, since it gives the maximum g-value anisotropy, Δg, per unit strain. The estimated values are

$$g_{3g} \geq 1.20 \quad \text{and} \quad g_{5g} \geq 42.4 \ . \tag{16}$$

Although a few films did not show any linewidth or line-shape anisotropy, which would imply a uniform strain across the film, the corresponding g_{3g} and g_{5g} values give only a lower limit: this is because the uncertainty introduced by the sliding effects discussed above prevents us from being certain of the actual deformation in each case.

The changes in the crystal field produced by the strains can be described by the following orbit-lattice Hamiltonian[3]

$$\mathcal{H}_{01} = \sum_{n,i,\alpha,\xi} G_i^{(n,\xi)} \epsilon_{i,\alpha} O_{i,\alpha}^{(n,\xi)} \ , \tag{17}$$

where $O_{i,\alpha}^{(n,\xi)}$ are linear combinations of the nth-order Steven's operators that transform like the normal strain $\epsilon_{i,\alpha}$, and the $G_i^{(n,\xi)}$ the orbit-lattice coupling parameters.

The change in the g value involves a second order of perturbation calculation in the orbit lattice and Zeeman interaction. Following Calvo *et al.*[3] the relative g shift for the [001] and [111] uniaxial strains can be written as

$$\frac{\Delta g}{g} = \frac{2G_{3g}^{(2)}\epsilon_{3g\theta}}{E_7 - E_8} \frac{\langle \Gamma_{7\alpha}|J_z|\Gamma_{8\mu}\rangle \langle \Gamma_{8\mu}|\frac{1}{2}[3J_z^2 - J(J+1)]|\Gamma_{7\alpha}\rangle}{\langle \Gamma_{7\alpha}|J_z|\Gamma_{7\alpha}\rangle} \frac{1}{2}(3\cos^2\theta - 1) \ , \tag{18}$$

and

$$\frac{\Delta g}{g} = \frac{3}{4} \frac{G_{5g}^{(2)}\epsilon_{5g}}{E_7 - E_8} \frac{\langle \Gamma_{7\beta}|J_+|\Gamma_{8\lambda}\rangle \langle \Gamma_{8\kappa}|J_+^2 - J_-^2|\Gamma_{7\beta}\rangle}{\langle \Gamma_{7\alpha}|J_z|\Gamma_{7\alpha}\rangle} \frac{1}{2}(3\cos^2\theta - 1) \ . \tag{19}$$

We have neglected terms with $l = 4, 6$ because they are expected to be at least one order of magnitude smaller than the second-order ones ($l = 2$); here we have assumed that the conduction electrons do not introduce drastic changes on those parameters. The lower limits for the tetragonal and trigonal second-order OLCP at unit strain were estimated for Au:Er and Ag:Er (see Table III) using Eqs. (19), (18), (15), and (16), the wave functions given by Lea, Leask, and Wolf[16] and the energy splitting between the Γ_7 ground state and the $\Gamma_8^{(i)}$ excited states given by Williams and Hirst.[9] These values are of the same order

TABLE III. Lower limits for the second-order OLCP of Er, Dy, and Yb in Au and Ag.

	Au:Er	Au:Yb	Ag:Er	Ag:Dy	PCM
$G_{3g}^{(2)}/\alpha_J$ (K)	≥ 515	≥ 449	≥ 200	≥ 137	1287
$G_{5g}^{(2)}/\alpha_J$ (K)	≥ 840	≥ 650	≤ -600	≤ -584	2574

of magnitude found for Au:Yb and Ag:Dy (Refs. 7 and 8) and are also in agreement with the second-order static crystalline field parameter found in hexagonal metals.[17] Recent magnetostriction experiments by Campbell *et al.*[18] confirm the values found for $G_{3g}^{(2)}/\alpha_J$ and $G_{5g}^{(2)}/\alpha_J$ in the case of Ag:Er. Our lower limit for the $G_{3g}^{(2)}/\alpha_J$ value is smaller than that given by Arbilly *et al.*[4] in the case of Ag:Er. Since both types of oriented films, i.e., (001) and (111), give the same g-value anisotropies for the NaCl substrate (see Fig. 6 and Table II), the structure of the film used to obtain the $G_{3g}^{(2)}/\alpha_J$ parameter has to be analyzed carefully: the lower limit could be overestimated if there are contributions from the (111) structure. This, together with the possible sliding of the film from the substrate could be the source of the different values obtained for the $G_{3g}^{(2)}/\alpha_J$ parameter.

V. CONCLUSIONS

The tetragonal and trigonal second-order OLCP were found to agree in sign with those predicted by the point-charge model (PCM)[2,7] in the case of Au:Er (see Table III), just as it was previously observed in Au:Yb.[8] This is surprising because it is well known from susceptibility experiments[9] that PCM does not explain the sign of the fourth-order static cubic-crystal-field parameter of rare-earth gold and silver diluted alloys, and d virtual-bound states (vbs) have been invoked to explain the sign of this parameter.[19] On the other hand, while the tetragonal second-order OLCP for Ag:Er [as in Ag:Dy (Ref. 7)] shows the same sign predicted by PCM, the trigonal OLCP shows the sign opposite to that predicted by PCM. This result together with the fact that Chow's[19] calculations can fit better the fourth-order static cubic crystal field for Au than for Ag, and that the positive g shift of Gd and Er in Ag are bigger than those in Au suggest that it might be necessary to improve the theoretical interpretation to understand the different crystal-field parameters measured in dilute alloys of rare earth in Au and Ag. These improvements would include shielding,[20] covalency effects,[9,21] and the influency of the vbs (p and/or d like) on the second-, fourth-, and sixth-order OLCP and fourth-order static cubic-crystal-field parameter. The width, splitting, and population of the vbs should also be considered in these calculations.

For the same reasons given in the case of Ag:Dy,[7] we believe that the $G_{3g}^{(2)}$ value for Ag:Er reported by Dodds and Sanny,[22] correspond to the $G_{5g}^{(2)}$ value.

Finally we want to comment on the nonuniformity of the normal strains across the film. From our experimental results we were able to get some idea about the strain distribution function $F(z)$ only in the case of trigonal distortions, therefore this distribution function will be given by $\epsilon_{5g}(z)/\epsilon_{5g}(z=0)$. The trial function [Eq. (4)] used to fit the data on Figs. 3 and 4 is just a simplified view of what we believe should happen for a nonuniform strain distribution across the film. We think that immediately after the interface the strain should be uniform, and probably the same happens at the end of the film, but with different intensities, allowing for some "relaxation" of the strains in between. We have approximated this behavior to the simple function of Eq. (4) with just three parameters. It could also be done with smoother functions but it would require more fitting parameters. The behavior commonly found in our experiments, of linewidth anisotropy with a little line-shape anisotropy, could be explained by the chosen function of Eq. (4) with $a=0$ and $c=\delta$, i.e., a linear decrease of the strain from the interface to the end of the film.

As far as the origin of the nonuniform strain distribution is concerned, we can say that it could be associated with the presence of a nonuniform distribution of dislocations across the film or to a true change in the lattice parameter. It will be interesting to do x-ray experiments at low temperature in order to get more information about the origin of the strain distribution across the film. Finally, it would also be interesting to find the theoretical strain distribution corresponding to a deformed film, by solving the equations of equilibrium with the boundary conditions appropriate to our experiment. This calculation is in progress at the present in our group, and will be published elsewhere.

ACKNOWLEDGMENT

This work has been partially supported by FAPESP and CNPq Brasil.

[1] R. Orbach and H. J. Stapleton, in *Electron Paramagnetic Resonance*, edited by S. Geschwind (Plenum, New York, 1972), p. 121, and references therein.

[2] Z. Sroubek, M. Tachiki, P. H. Zimmermann, and R. Orbach, Phys. Rev. 165, 435 (1968).

[3] R. Calvo, S. B. Oseroff, C. Fainstein, M. C. G. Passeggi, and M. Tovar, Phys. Rev. B 9, 4888 (1974).

[4] D. Arbilly, G. Deutscher, E. Grumbaum, R. Orbach, and J. T. Suss, Phys. Rev. B 12, 5068 (1975).

[5] J. F. Suassuna, G. E. Barberis, C. Rettori, and C. A. Pelá, Solid State Commun. 22, 347 (1977).

[6] G. E. Barberis, J. F. Suassuna, C. Rettori, and C. A. Pelá,

Solid State Commun. 23, 603 (1977).
[7]C. A. Pelá, G. E. Barberis, J. F. Suassuna, and C. Rettori, Phys. Rev. B 21, 34 (1980).
[8]F. G. Gandra, C. A. Pelá, G. E. Barberis, D. Davidov, and C. Rettori, Phys. Rev. B (in press).
[9]G. Williams and L. L. Hirst, Phys. Rev. 185, 407 (1969).
[10]J. F. Suassuna, Ph.D. thesis (UNICAMP, Brasil) (unpublished).
[11]C. A. Pelá, Ph.D. thesis (UNICAMP, Brasil) (unpublished).
[12]L. J. Tao, D. Davidov, R. Orbach, and E. P. Chock, Phys. Rev. B 4, 5 (1971).
[13]R. Chui, R. Orbach, and B. L. Gehman, Phys. Rev. B 2, 2298 (1970).
[14]*American Handbook of Physics,* 2nd ed. (McGraw-Hill, New York, 1963).
[15]M. Peter, D. Shaltiel, J. H. Wernick, H. J. Williams, J. B. Mock, and R. C. Sherwood, Phys. Rev. 126, 1395 (1962).
[16]K. R. Lea, M. J. M. Leask, and W. P. Wolf, J. Phys. Chem. Solids 23, 1381 (1962).
[17]P. Touborg and J. Hog, Phys. Rev. Lett. 33, 775 (1974).
[18]I. A. Campbell, G. Creuzet, and J. Sanchez, Phys. Rev. Lett. 43, 234 (1979).
[19]H. C. Chow, Phys. Rev. B 7, 3404 (1973); J. M. Dixon and R. Dupree, J. Phys. F 1, 539 (1971).
[20]G. Burns, J. Chem. Phys. 42, 377 (1965).
[21]B. Bleaney, Proc. R. Soc. London Ser. A 277, 289 (1964).
[22]S. A. Dodds and J. Sanny, Phys. Rev. B 18, 39 (1978).